THE EUROPEAN
PHYSICAL JOURNAL C

CrossMark

From sine-Gordon to vacuumless systems in flat and curved spacetimes

D. Bazeia[a], **D. C. Moreira**

Departamento de Física, Universidade Federal da Paraíba, João Pessoa, PB 58051-970, Brazil

Abstract In this work we start from the Higgs prototype model to introduce a new model, which makes a smooth transition between systems with well-located minima and systems that support no minima at all. We implement this possibility using the deformation procedure, which allows the obtaining a sine-Gordon-like model, controlled by a real parameter that gives rise to a family of models, reproducing the sine-Gordon and the so-called vacuumless models. We also study the thick brane scenarios associated with these models and investigate their stability and renormalization group flow. In particular, it is shown how gravity can change from the 5-dimensional warped geometry with a single extra dimension of infinite extent to the conventional 5-dimensional Minkowski geometry.

1 Introduction

Topological solutions in field theory are related to many phenomena in physics [1–3]. In particular, when we have models in 1+1 dimensions involving a potential written in terms of a scalar field and with a set of degenerate minima, such solutions represent transitions between consecutive minima and are called *kinks*. The minima define the possible vacuum states at the quantum level, and they are distributed over the many values for the field. Such distribution can appear in the most diverse ways, for instance, in the ϕ^4-model one has only one topological sector, defined between two consecutive minima, while in the sine-Gordon model [4] one has an infinite copy of the same sector, always between two consecutive and well-localized minima. A system that is quite different in this perspective is the vacuumless model [5,6]. In this model we still have a topological sector, which can be interpreted as connecting two minima of the scalar potential, but now they are located at infinity. In this case, the field solution is asymptotically divergent and has infinite ampli-

tude, but keeps its topological character well behaved [7]. It is worth mentioning that vacuumless systems appear in a diversity of contexts in high energy physics [5–11].

The aim of this paper is to construct a model that, with the proper variation of a given parameter, makes the transition between systems with well-located minima and systems that support no minima at all. The model presented here has as limit cases the sine-Gordon and the vacuumless models. Using the deformation procedure developed in Ref. [12], we find a field transformation that takes us to a new system with a double sine-Gordon-like behavior, which has two infinitely degenerate sets of solutions. One of these sets transits between the sine-Gordon kink and the vacuumless solution. The second set coincides with the previous one in one of its limits and, except from a phase, in the other limit case it is destroyed, remaining only the zero-energy solutions. Thus, in one of the limits of the model the two phases coincide, generating infinite copies of the same topological sector, and in the other limit only one topological sector survives.

Models in field theory motivate generalizations of the Randall–Sundrum model [13,14] in the presence of scalar fields [15–24], which are known as *thick branes*. For this reason, in this work we also study the thick brane scenario generated by the scalar field model which we first introduce and study in the flat spacetime. In particular, we find a brane that transits between the sine-Gordon brane [18] and a flat 5-dimensional spacetime with two zero-energy solutions for the scalar field. The idea here is similar to the case investigated in [25], in which the authors propose a braneworld scenario where the brane changes from a thick to a thin behavior. In the current study, however, we describe a mechanism in which a single parameter can be used to control the brane profile, contributing to change the 5-dimensional warped geometry into a flat geometry.

Although the braneworld model that we explore below is more involved, it also supports analytical solutions. Thus, in the 5-dimensional spacetime with a single extra dimen-

[a] e-mail: bazeia@fisica.ufpb.br

sion of infinite extent, we also analyze the stability of the braneworld scenario against tensorial perturbations. In the sense of gauge/gravity duality [26–30], where the extra dimension can be identified with the energy scale of the holographic dual field theory, we also study its implications for the renormalization group flow (the RG flow) in the dual field theory, since stability of the gravitational sector has relevant information as regards the dual model [31].

The subject to be explored in the current work is organized as follows. In Sect. 2 we review several aspects of the first-order formalism for a single real scalar field and its relationship with the Bogomol'nyi–Prasad–Somerfield (BPS) solutions [32,33]. Then we discuss the deformation procedure and show how it acts to generate the new model in the 2-dimensional spacetime. We go on and study in Sect. 3 the new model and its topological solutions, including how the energy and energy density behave. In addition, we also show that the solutions obtained are stable. Moreover, in Sect. 4 we analyze the properties of the thick branes that can be constructed from the model. We also investigate stability of the brane against metric fluctuations and study implications of the RG flow for the dual field theory. We end the work in Sect. 5, adding some comments and conclusions.

2 Generalities

2.1 First-order formalism

The behavior of a scalar field is usually encoded in a Lagrangian density having the general form

$$\mathcal{L}(\phi, \partial_\mu \phi) = \frac{1}{2} \partial_\mu \phi \partial^\mu \phi - V(\phi). \tag{1}$$

Here ϕ is the scalar field and $V(\phi)$ is the potential of the model, which determines how the field behaves. In the flat spacetime with (1, 1) spacetime dimensions, the metric tensor becomes $\eta_{\mu\nu} = \mathrm{diag}(1, -1)$, so the scalar field only depends on the two coordinates x and t, i.e., $\phi = \phi(x, t)$. For simplicity, we also work with dimensionless fields and coordinates. The equation of motion for the scalar field derived from the Lagrangian (1) is given by

$$\partial_\mu \partial^\mu \phi + \frac{\mathrm{d}V}{\mathrm{d}\phi} = 0. \tag{2}$$

As the Lagrangian (1) is Lorentz invariant, we can focus on static solutions, since traveling waves can be obtained from a Lorentz boost. For static configurations Eq. (2) becomes a second-order differential equation given by

$$\frac{\mathrm{d}^2 \phi}{\mathrm{d}x^2} = \frac{\mathrm{d}V}{\mathrm{d}\phi}. \tag{3}$$

Another important quantity we are interested in is the energy-momentum tensor

$$T^{\mu\nu} = \partial^\mu \phi \partial^\nu \phi - \eta^{\mu\nu} \mathcal{L}. \tag{4}$$

In particular, its T^{00} component provides the energy density of the solution we are looking for. We represent it by $\rho(x)$, which is explicitly given by

$$\rho(x) = \frac{1}{2} \phi'^2 + V(\phi) \tag{5a}$$

$$= \frac{1}{2} \left(\phi' \mp \sqrt{2V(\phi)} \right)^2 \pm \phi' \sqrt{2V(\phi)}. \tag{5b}$$

Note that, for positive-definite energy, the potential must be non-negative, i.e., $V(\phi) \geq 0$. A powerful tool in the treatment of these models is the use of an auxiliary function, denoted by $W(\phi)$, which is introduced as follows:

$$V(\phi) = \frac{1}{2} W_\phi^2, \tag{6}$$

where $W_\phi = \mathrm{d}W/\mathrm{d}\phi$. In this case the expression for the energy density (5a) becomes

$$\rho(x) = \frac{1}{2} \left(\phi' \mp W_\phi \right)^2 \pm \frac{\mathrm{d}W}{\mathrm{d}x} \tag{7}$$

and Eq. (3) can now be given as the first-order differential equations

$$\frac{\mathrm{d}\phi}{\mathrm{d}x} = \pm W_\phi. \tag{8}$$

It implies that the quadratic term in (7) disappears and, as a consequence, the energy density is only related to the x-derivative of W. Thus, the energy of the model is determined only by the asymptotic behavior of the function W in the coordinate space; that is, one can write

$$E_{\mathrm{BPS}} = \int_{-\infty}^{\infty} \rho(x) \, \mathrm{d}x$$
$$= |W(\phi(\infty)) - W(\phi(-\infty))|. \tag{9}$$

In this case the energy (9) is called BPS energy [32,33].

Relevant phenomena occur when the system under analysis presents a set of degenerate minima. In these situations each pair of consecutive minima form distinct topological sectors that, in turn, have different solutions. These solutions are called *kinks*. The simplest case of models having such properties is the well-known Higgs prototype or ϕ^4-model, defined by the potential

$$V(\phi) = \frac{1}{2} (1 - \phi^2)^2, \tag{10}$$

which has two degenerate minima at $\phi = \pm 1$ and a topological sector having a kink solution given explicitly by $\phi(x) = \tanh(x)$.

An interesting way to characterize a kink is the existence of a topological current. Here, we define it by [7]

$$j^\mu = \epsilon^{\mu\nu}\partial_\nu W(\phi(x)), \tag{11}$$

where $\epsilon^{\mu\nu}$ is the antisymmetric symbol in two dimensions with $\epsilon^{01} = 1$. Associated with this current (11) we have a topological charge given by

$$Q = \int_{-\infty}^{\infty} j^0 \mathrm{d}x = W(\phi(\infty)) - W(\phi(-\infty)). \tag{12}$$

Despite the similarities in the values of the charge (12) and the BPS energy (9), they have fundamental differences. While the BPS energy is associated with a continuous symmetry and can be identified from the Noether theorem, the charge (12) is associated with the topology of each solution, and results from the transition of the topological solution in between two minima of the potential.

2.2 The deformation procedure

Once we know the behavior of a given model, with its characteristics and general behavior, it is interesting to look for new well-behaved models. In this sense, the deformation method [12] is a powerful tool to find new models in field theory. The method consists of choosing a theory with the Lagrangian $\mathcal{L}(\phi, \partial_\mu\phi)$ having the form (1) and then perform a transformation of the type

$$\phi \to f(\chi). \tag{13}$$

We then get

$$\mathcal{L}(\phi, \partial_\mu\phi) = f_\chi^2 \, \mathcal{L}(\chi, \partial_\mu\chi) \tag{14}$$

where

$$\mathcal{L}(\chi, \partial_\mu\chi) = \frac{1}{2}\partial_\mu\chi\partial^\mu\chi - U(\chi), \tag{15}$$

with the potential $U(\chi)$ given by

$$U(\chi) = \frac{V(\phi \to f(\chi))}{f_\chi^2}. \tag{16}$$

This is a field redefinition, but if we consider the model (15) described by the potential (16) as a new model, and call it the deformed model, in this case there is a $\bar{W}$ function such that the first-order differential equations

$$\frac{\mathrm{d}\chi}{\mathrm{d}x} = \bar{W}_\chi, \tag{17}$$

with $\bar{W}_\chi = W_\phi(\phi \to f(\chi))/f_\chi$, provide solutions for the field $\chi(x)$. In particular, among the characteristics of the new

model, we can highlight that the total energy of the solution is

$$E = |\bar{W}(\chi(\infty)) - \bar{W}(\chi(-\infty))|, \tag{18}$$

since the deformed model also has a first-order structure. However, the deformed model engenders another important property: the transformation (13) allows us to find the solution for the field $\chi(x)$ without the need to deal directly with Eq. (17). What we have is that the solution to the new field is obtained by inverting the transformation (13). Thus, one finds

$$\chi(x) = f^{-1}(\phi(x)), \tag{19}$$

where $\phi(x)$ represents a solution for the previous model. In this sense, Eq. (19) represents the main link between the ϕ-model and the deformed χ-model. For more details, see [12].

3 Model

In this work we follow the deformation procedure and introduce a new model generated by the deformation function

$$f_\lambda(\chi) = \tanh\left(\frac{1}{\theta\sqrt{2-\theta^2}}\tanh^{-1}\left(\theta\frac{\mathrm{sc}(\chi,\lambda)}{\sqrt{2-\theta^2}}\right)\right) \tag{20}$$

which is applied to the ϕ^4 model (10). Here θ is a real parameter ($\neq \pm\sqrt{2}$) and the function $\mathrm{sc}^{-1}(\chi, \lambda)$ is one of the Jacobi elliptic functions, defined by the ratio

$$\mathrm{sc}(\chi, \lambda) = \frac{\mathrm{sn}(\chi, \lambda)}{\mathrm{cn}(\chi, \lambda)}, \tag{21}$$

where $\mathrm{sn}(\chi, \lambda)$ and $\mathrm{cn}(\chi, \lambda)$ are the Jacobi elliptic sine and cosine, respectively. Here we have

$$\mathrm{cn}^2(\chi, \lambda) + \mathrm{sn}^2(\chi, \lambda) = 1, \tag{22a}$$
$$\mathrm{dn}^2(\chi, \lambda) + \lambda\mathrm{sn}^2(\chi, \lambda) = 1, \tag{22b}$$

where λ is a parameter in the interval $[0, 1]$. In particular for $\lambda = 0$ we have $\mathrm{sn}(\chi, 0) = \sin(\chi)$, $\mathrm{cn}(\chi, 0) = \cos(\chi)$ and $\mathrm{dn}(\chi, 0) = 1$, where we retrieve the basic trigonometric relations, and for $\lambda = 1$ we have $\mathrm{sn}(\chi, 1) = \tanh(\chi)$ and $\mathrm{cn}(\chi, 1) = \mathrm{dn}(\chi, 1) = \mathrm{sech}(\chi)$, which lead us to the hyperbolic functions. The new model found from the deformation function (20) and the potential (10) is

$$U(\chi, \lambda) = \frac{1}{2}\frac{\left(2\mathrm{cn}^2(\chi, \lambda) - \theta^2\right)^2}{\mathrm{dn}^2(\chi, \lambda)}. \tag{23}$$

Its behavior is depicted in Fig. 1. The potential (23) has $\mathbb{Z}_2$-symmetry and is invariant under transformation $\phi \to \phi + 2K_\lambda$, where $K_\lambda = \mathrm{cn}^{-1}(0, \lambda)$. In this case we find
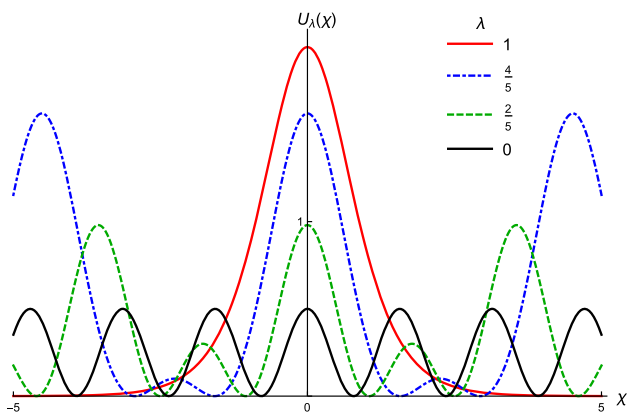
Fig. 1 The potential (23) for some values of λ and $\theta^2 = 1 - \lambda$. As λ increases in the interval [0, 1], the model evolves from the sine-Gordon model at $\lambda = 0$ to a double sine-Gordon model and finally to the vacuumless model, at $\lambda = 1$

$W_\chi = \pm(2\text{cn}^2(\chi, \lambda) - \theta^2)/\text{dn}(\chi, \lambda)$, which implies that the W function of the model is

$$W(\chi, \lambda) = \frac{2}{\lambda}\left(\text{am}(\chi, \lambda) - \sqrt{1-\lambda}\tan^{-1}(\sqrt{1-\lambda}\text{sc}\,(\chi, \lambda))\right)$$
$$- \frac{\theta^2 \cos^{-1}(\text{cd}(\chi, \lambda)\sqrt{1 - \text{cd}^2(\chi, \lambda)}\text{dn}(\chi, \lambda)}{(1-\lambda)\text{sn}(\chi, \lambda)}, \quad (24)$$

where $\text{am}(\chi, \lambda) = d\,(\text{dn}(\chi, \lambda))\,/d\chi$ is the *Jacobi amplitude*. Although we initially present the model with two parameters, we are interested in situations where only one parameter is necessary to describe the changes in the model. So we assume that $\theta = \theta(\lambda)$. We also impose on $\theta(\lambda)$ the conditions $\theta(0) = 1$ and $\theta(1) = 0$ in order to find the vacuumless model [7] for $\lambda = 1$ and the sine-Gordon model [4] for $\lambda = 0$. As a consequence we obtain the particular cases $W(\chi, 1) = 4\tan^{-1}(e^\chi) - \pi$ and $W(\chi, 0) = \sin(2\chi)/2$, so the sine-Gordon and vacuumless models appear in the system as

$$U(\chi, 0) = \frac{1}{2}\cos^2(2\chi), \quad (25a)$$

$$U(\chi, 1) = 2\,\text{sech}^2(\chi). \quad (25b)$$

The parameter λ has an interesting behavior: when it increases from 0 to unity, the model changes from the sine-Gordon to the vacuumless model. Physically, it transforms the periodic sine-Gordon potential (25) to a non-periodic one, the hyperbolic potential (25b) which defines the vacuumless model. The distinct solutions appear in Fig. 2 and in Fig. 3 one illustrates how the energy density becomes more and more diffuse, as λ increases from zero to unity.

Once the model has been presented, we must solve the first-order equation

$$\chi' = \frac{2\text{cn}(\chi, \lambda)^2 - \theta^2}{\text{dn}(\chi, \lambda)}. \quad (26)$$
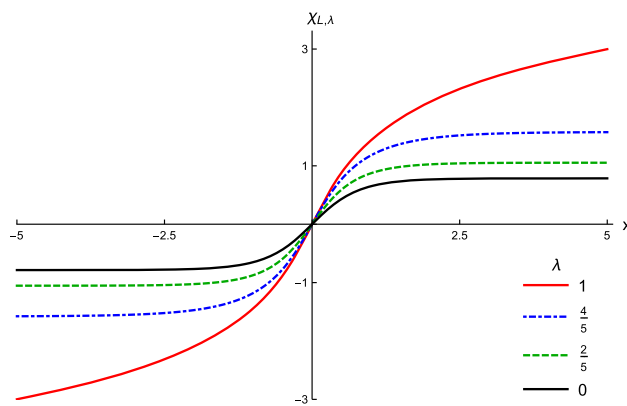

Fig. 2 The solution $\chi_{L,\lambda}$ for some values of λ and $\theta^2 = 1 - \lambda$. Here we observe how the large kink of the model evolves from the sine Gordon kink to the vacuumless solution

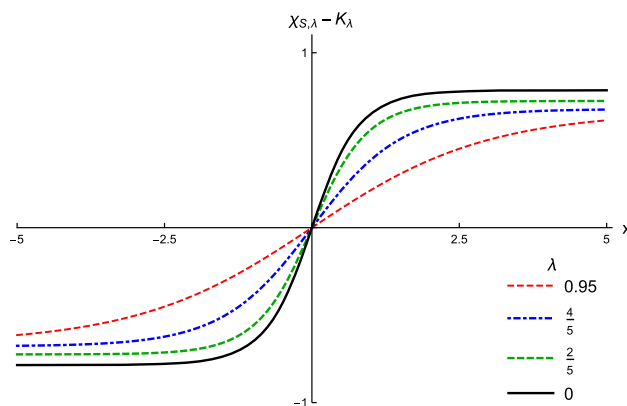**Fig. 3** The solution $\chi_{S,\lambda} - K_\lambda$ for some values of λ and $\theta^2 = 1 - \lambda$. Here we observe how the small kink tends to disappear in the limit $\lambda \to 1$

Equation (26) has two infinite set of solutions. The first one we call *large kinks* and they are given by

$$\chi_{L,\lambda}(x) = \text{sc}^{-1}\left(\frac{\sqrt{2 - \theta^2}}{\theta}\tanh\left(\theta\sqrt{2 - \theta^2}x\right), \lambda\right) + 2n\text{K}_\lambda. \quad (27)$$

The behavior of the solution (27) is depicted in Fig. 2 for $n = 0$. It asymptotically approaches $\chi_{L,\lambda}(\pm\infty) = \pm\text{sc}^{-1}(\sqrt{2 - \theta^2}/\theta, \lambda)$ and in the vicinity of the origin behaves like $\chi_{L,\lambda}(x \simeq 0) \simeq (2 - \theta^2)x + \mathcal{O}(x^2)$. We note that, as $\theta \to 0$, $\chi_{L,\lambda}(\pm\infty)$ tends to diverge and $\chi_{L,\lambda}(x \simeq 0)$ remains well behaved. For $\theta \to 1$ we do not have pathologies in the solution. Thus, the large kink describes, as a function of the λ parameter, systems that transit between the sine-Gordon kink and the vacuumless solution. Particularly, we have

$$\chi_{L,1}(x) = \sinh^{-1}(2x)\ \text{(vacuumless solution)}; \quad (28a)$$

$$\chi_{L,0}(x) = \tan^{-1}(\tanh(x))\ \text{(sine-Gordon kink)}. \quad (28b)$$

The second set of solutions we find from Eq. (26) is

$$\chi_{S,\lambda}(x) = \text{sc}^{-1}\left(\frac{\theta \tanh\left(\theta\sqrt{2-\theta^2}x\right)}{\sqrt{(2-\theta^2)(1-\lambda)}}, k\right) + (2n+1)\text{K}_\lambda,$$

(29)

and we call it a *small kink*. Its shape is depicted in Fig. 3 for $n = 0$, except for the phase K_λ. The solution (29) asymptotically approaches $\chi_{S,\lambda}(\pm\infty) = \pm\text{sc}^{-1}(\theta/\sqrt{(2-\theta^2)(1-\lambda)}, \lambda) + K_\lambda$ and in the neighborhoods of $x = 0$ behaves as $\chi_{S,\lambda}(x \simeq 0) \simeq K_\lambda + \theta^2 x/\sqrt{1-\lambda} + \mathcal{O}(x^2)$. The small kink has a phase K_λ, which causes its topological sector to move away from the center of the potential (23) to infinity as $\lambda \to 1$. With a suitable choice for $\theta(\lambda)$ we can destroy the topological sectors associated with small kinks when $\lambda = 1$. Thus, only the topological sector of the vacuumless solution remains at that point. If we drop the phase in the small kink (29), it is possible to note that the zero-energy solutions also remain, but at infinity. A simple choice in this direction that also obeys the conditions $(\theta(0), \theta(1)) = (1, 0)$ is $\theta(\lambda) = \sqrt{1-\lambda}$. With this choice for $\theta(\lambda)$ we can explicitly rewrite the solutions of large and small kinks as

$$\chi_{L,\lambda}(x) = \text{sc}^{-1}\left(\sqrt{\frac{1+\lambda}{1-\lambda}}\tanh(\sqrt{1-\lambda^2}x), \lambda\right),$$

(30a)

$$\chi_{S,\lambda}(x) = \text{sc}^{-1}\left(\frac{\tanh\left(\sqrt{1-\lambda^2}x\right)}{\sqrt{1+\lambda}}, \lambda\right) + K_\lambda.$$

(30b)

So now we have a double sine-Gordon-like model with two field solutions coming from the two manifest topological sectors. Both kinks retrieve the sine-Gordon solution when $\lambda = 0$, but as λ grows, such solutions have distinct properties. Large kink becomes more diffuse until reaching the solution of the vacuumless model, which has divergent amplitude. It implies that at this point all topological sectors of the model are sent to infinity, except for the sector that is at the center of the potential (23). A small kink also becomes more diffuse as $\lambda \to 1$, but it is destroyed when $\lambda = 1$. As we shall see later, it happens because as the associated topological sector moves away from the center of the potential its energy approaches zero. Moreover, one can show that the mass of the meson in the minima of the potential is given by $m_\lambda^2 = U''(\chi = \chi_{\min}) = 4(1-\lambda^2)$, where $\chi_{\min}$ is a minimum of (23). Here, we choose to write the model in terms of that quantity, whenever possible.

We can now perform the analysis of the energy densities of the model. The energy density of the large kink (27) is given by
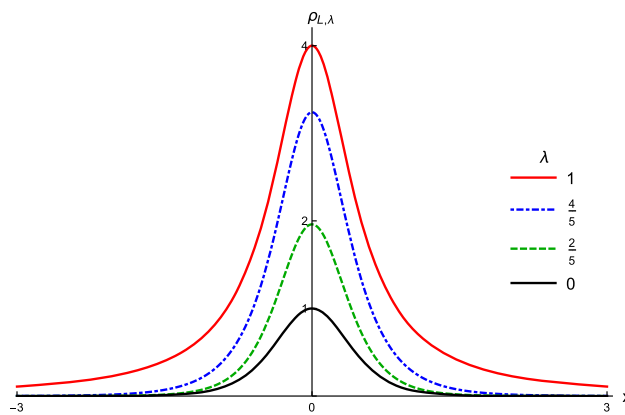

Fig. 4 The energy density (31) for some values of λ. Here one notes how $\rho_{L,\lambda}$ behaves as $\lambda \to 1$, becoming more diffuse but keeping its localized profile

$$\rho_{L,\lambda}(x) = \frac{(1-\lambda)(1+\lambda)^2\text{sech}^2\left(\frac{m_\lambda}{2}x\right)}{(\cosh(m_\lambda x) - \lambda)\left((1+\lambda)\tanh^2\left(\frac{m_\lambda}{2}x\right)+1\right)}$$

(31)

and its shape is depicted in Fig. 4. It makes the transition between the curves $\rho_{L,1}(x) = 4/(1+4x^2)$ and $\rho_{L,0}(x) = \text{sech}^2(2x)$. Asymptotically Eq. (31) decays as $\rho_{L,\lambda}(x \to \infty) \simeq 8(1-\lambda)(1+\lambda)^2 e^{-2m_\lambda x}/(2+\lambda) + \mathcal{O}(e^{-4m_\lambda x})$, where we found the particular case $\rho_{L,0}(x \to \infty) \simeq 4e^{-4x}$. We do not have information for the case $\lambda = 1$ in the general asymptotic expansion for the energy density, but a direct approach in $\rho_{L,1}(x)$ leads to the expression $\rho_{L,1}(x \to \infty) \simeq 1/x^2 + \mathcal{O}(x^{-4})$, which decays much slower than the exponential. This change in the asymptotic behavior is due to the mass scale of the quantum meson which, for $\lambda = 1$, is zero. On the other hand the behavior of (31) in the vicinity of $x = 0$ is given by $\rho_{L,\lambda}(x \simeq 0) \simeq (1+\lambda)^2 - (1+\lambda)^3(4-\lambda^2-\lambda)x^2 + \mathcal{O}(x^3)$, which shows that the central portions of the energy density increases and becomes a bit more concentrated as $\lambda \to 1$.

For the small kink we have the energy density given by

$$\rho_{S,\lambda}(x) = \frac{(1-\lambda)(1+\lambda)^2\text{sech}^2\left(\frac{m_\lambda}{2}x\right)}{(\cosh(m_\lambda x) + \lambda)\left(\tanh^2\left(\frac{m_\lambda}{2}x\right)+1+\lambda\right)}$$

(32)

and its behavior is depicted in Fig. 5. Equation (32) transits between the curves $\rho_{S,1}(x) = 0$ and $\rho_{L,0}(x) = \text{sech}^2(2x)$. Asymptotically it decay as $\rho_{S,\lambda}(x \to \infty) \simeq 8(1-\lambda)(1+\lambda)^2 e^{-2m_\lambda x}/(2+\lambda) + \mathcal{O}(e^{-4m_\lambda x})$, revealing that we cannot distinguish the energy densities of the fields (27) and (29) when $x \to \infty$. For $x \simeq 0$ we have $\rho_{S,\lambda}(x \simeq 0) \simeq (1-\lambda) - (1-\lambda)^2(\lambda+4)x^2 + \mathcal{O}(x^3)$. It shows that, despite the similar asymptotic behavior (for $\lambda \neq 1$), the evolution of (31) and (32) in terms of the parameter λ is very different. The height and width of the energy density (31) grow with λ, becoming more diffuse but still with a localized pro-
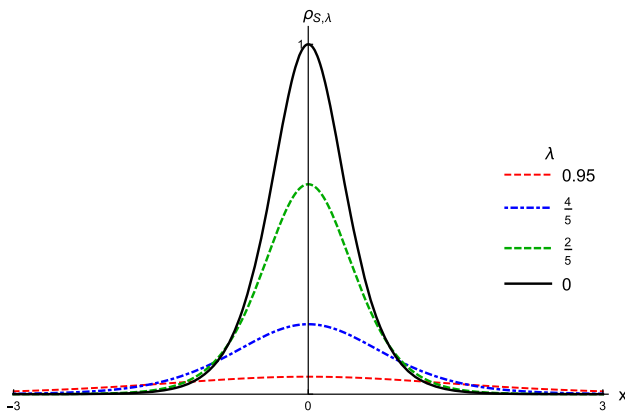
Fig. 5 The energy density (32) for some values of λ. Here one notes how $\rho_{S,\lambda}$ behaves as $\lambda \to 1$, becoming more delocalized, disappearing at $\lambda = 1$

Fig. 6 The energy behavior as a function of λ. Here we observe that $E_L(\lambda)$ evolves from $E_L(0) = 1$ to $E_L(1) = 2\pi$ and $E_S(\lambda)$ decreases from $E_S(0) = 1$ to $E_S(1) = 0$

file. Meanwhile, as λ grows, the width of the energy density (32) increases, but its central portion decreases and becomes less concentrated, which implies that as the solution evolves it becomes more diffuse, but also delocalized. As a consequence, the area under the energy density (32) become smaller until it disappears, at $\lambda = 1$.

Integrating (31) and (32) we find the energy of large and small kinks, given by

$$
E_L(\lambda) = \frac{2}{\lambda}\left(2\tan^{-1}\left(\sqrt{\frac{1+\lambda}{1-\lambda}} \right) \right.
$$
$$
\left. -\sqrt{1-\lambda}\,(2+\lambda)\tan^{-1}\left(\sqrt{1+\lambda} \right) \right) \tag{33}
$$

and

$$
E_S(\lambda) = -\frac{2}{\lambda}\left(2\cot^{-1}\left(\sqrt{\frac{1+\lambda}{1-\lambda}} \right) \right.
$$
$$
\left. -\sqrt{1-\lambda}\,(2+\lambda)\cot^{-1}\left(\sqrt{1+\lambda} \right) \right), \tag{34}
$$

respectively. The corresponding behaviors are depicted in Fig. 6. Here one observes that the energy of the solutions (27) and (29) are bounded. Equation (33) is a monotonically increasing function of the λ parameter confined in the interval $[1, 2\pi]$, where $E_L(0) = 1$ and $E_L(1) = 2\pi$, and Eq. (34) is a monotonically decreasing function of the λ parameter confined in the interval $[0, 1]$, with $E_S(0) = 1$ and $E_S(1) = 0$. Moreover, it is easy to show that (33) and (34) are related by $E_L(\lambda) = E_S(\lambda) + \frac{\pi}{\lambda}\left(2 - (2+\lambda)\sqrt{1-\lambda} \right)$.

3.1 Linear stability

In this section we analyze the stability of the solutions of the models presented so far. The usual procedure is to take a time-dependent perturbation around the static solution written in the form $\chi(x, t) = \chi(x) + \sum_n \eta_n(x)\cos(\omega_n t)$, for small $\eta_n(x)$, and then insert $\chi(x, t)$ into (2). The procedure gives
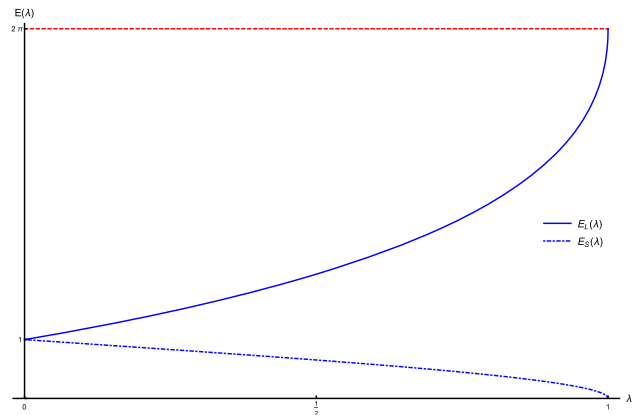
$$
\left(-\frac{d^2}{dx^2} + v(x) \right) \eta_n(x) = \omega_n^2 \eta_n(x), \tag{35}
$$

which is a Schrödinger-like equation with a stability potential given by

$$
v(x) = \left. \frac{d^2 U}{d\chi^2} \right|_{\chi=\chi(x)} \tag{36a}
$$
$$
= \bar{W}_{\chi\chi}^2 \big|_{\chi=\chi(x)} + \bar{W}_{\chi\chi\chi}\bar{W}_\chi \big|_{\chi=\chi(x)}. \tag{36b}
$$

Inserting the large kink solution (27) into (36) we find

$$
v_{L,\lambda}(x) = \frac{1-\lambda^2}{(\cosh(m_\lambda x) - \lambda)^2((1+\lambda)\tanh^2\left(\frac{m_\lambda}{2}x \right) + 1)^2}
$$
$$
\times \left[2(2+\lambda)^2\left(\cosh(2m_\lambda x) - \frac{\lambda(\lambda+7)+8}{2+\lambda}\cosh(m_\lambda x) \right) \right.
$$
$$
- (1+\lambda)^2\left((1+\lambda)(\lambda+4)\mathrm{sech}^2\left(\frac{m_\lambda}{2}x \right) - 6\lambda \right)
$$
$$
\left. \times \mathrm{sech}^2\left(\frac{m_\lambda}{2}x \right) + \lambda(\lambda(\lambda(\lambda+2)+19)+48)+24 \right], \tag{37}
$$

which is depicted in Fig. 7. For $\lambda = 1$ we have $v_{L,1}(x) = 4\left(8x^2 - 1 \right)/\left(4x^2 + 1 \right)^2$, which is a volcano potential, and for $\lambda = 0$ we have $v_{L,0}(x) = 4 - 8\mathrm{sech}^2(2x)$, which is a reflectionless potential. Equation (37) has a global minimum at $v_{L,\lambda}(0) = (1+\lambda)\left(\lambda^2 + \lambda - 4 \right)$; this minimum increases or decreases, depending on λ being above or below the point at $\tilde{\lambda} = \frac{1}{3}\left(\sqrt{13} - 2 \right)$. It shows that the potential (37), as λ grows, becomes deeper and after $\lambda = \tilde{\lambda}$ it comes back to its initial depth.

The change in the shape of the stability potential, in this case, is due to the behavior of the meson mass in the minima of (23). As $\lambda \to 1$ we have $m_\lambda^2 \to 0$. Note that $v_{L,\lambda}(0) < 0$ for all λ and translational invariance requires the existence of at least one bound state, so the transition between the reflectionless and the volcano shapes in this case describes the tran-
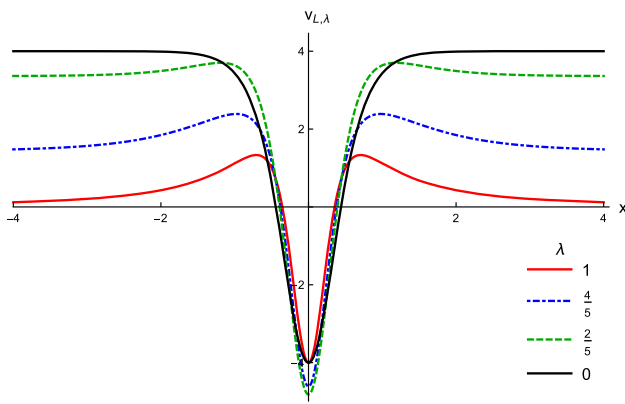
Fig. 7 The stability potential $v_{L,\lambda}(x)$ given by (37) for some values of λ. When $\lambda = 0$, we have a reflectionless potential and as λ increases the shape of the potential changes to become of the volcano type

sition from systems with massive meson to systems having a massless meson. This is another relevant physical behavior induced by the parameter λ, which will lead to distinct possibilities when used to describe braneworld scenarios, as we discuss in Sect. 4.

Now, inserting the small kink solution (29) in the general expression for the stability potential (36), we find

$$
\begin{aligned}
v_{S,\lambda}(x) = {} & \frac{1-\lambda^2}{(\cosh(m_\lambda x)+\lambda)^2(\tanh^2(\sqrt{1-\lambda^2}x)+1+\lambda)^2} \\
& \times \Bigg[2(2+\lambda)^2\left(\cosh(2m_\lambda x) - \frac{(1-\lambda)\lambda+8}{2+\lambda}\cosh(m_\lambda x)\right) \\
& - 2\lambda\left(\lambda\left(\lambda^2+\lambda-1\right)+3\right)\operatorname{sech}^2\left(\frac{m_\lambda}{2}x\right) \\
& - \left(\lambda^3-5\lambda+4\right)\operatorname{sech}^4\left(\frac{m_\lambda}{2}x\right) - \lambda^2(21-(\lambda-6)\lambda)+24\Bigg],
\end{aligned}
$$

$$(38)$$

which is depicted in Fig. 8. For $\lambda = 1$ we have $v_{S,1} = 0$ and for $\lambda = 0$ we have $v_{S,0} = 4 - 8\operatorname{sech}^2(2x)$, as expected. At the center we have $v_{S,\lambda}(0) = (\lambda - 1)(\lambda + 4)$, showing
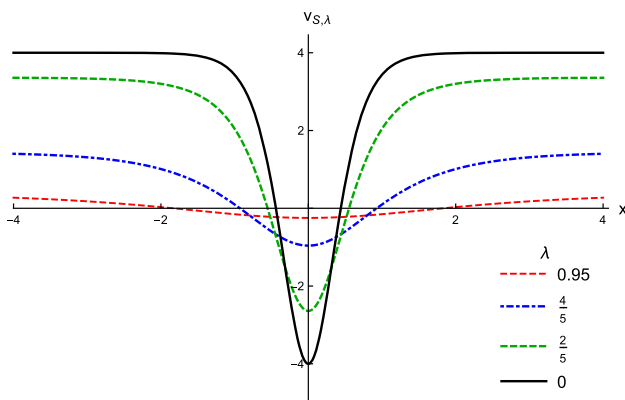

Fig. 8 The stability potential $v_{S,\lambda}(x)$ (38) for some values of λ. Here we observe that, as λ increases, its depth diminishes and disappears at $\lambda = 1$

that the potential (38) becomes shallower as λ grows, finally disappearing when $\lambda = 1$. Now, as λ grows, the stability potential keeps its reflectionless shape. As a consequence, the bound states of (38) become less pronounced as $\lambda \to 1$ and they disappear when $\lambda = 1$.

Asymptotically, both (37) and (38) approach $v_{L,\lambda}(\pm\infty) = v_{S,\lambda}(\pm\infty) = m_\lambda^2$. Moreover, one notes that the Hamiltonian $H = -\mathrm{d}^2/\mathrm{d}x^2 + v(x)$ can be rewritten as $H = S^\dagger S$ with $S^\dagger = -\mathrm{d}/\mathrm{d}x - W_{\phi\phi}$ by using Eq. (12). Thus we have $\omega_n^2 \geq 0$ for all values of n, since H is non-negative. As Eq. (35) does not admit negative energy modes, the stability of the solution is then ensured.

The translational invariance of the solutions we presented so far implies the existence of at least one bound state for each topological sector, which is given by the zero mode of Eq. (35). In the formula, if we represent the zero mode by $\eta_0(x)$, it is the derivative of the field solution,

$$
\eta_0(x) = \frac{\mathrm{d}\chi}{\mathrm{d}x}. \tag{39}
$$

For large and small kinks the shapes are depicted in Fig. 9, where one can observe how (37) holds the nice behavior of its zero mode, and how the zero mode of (38) gets smaller until it disappears when $\lambda = 1$.

4 Braneworld

Models described by scalar fields have direct applications in gravitation, providing braneworld scenarios for thick branes. In this context, the scalar field acts as a source of gravity around the brane, and thus describes how gravity behaves throughout the bulk. The system we are interested consists of a 3-brane embedded in a (4+1) spacetime with an extra dimension of infinite extent. The background geometry can
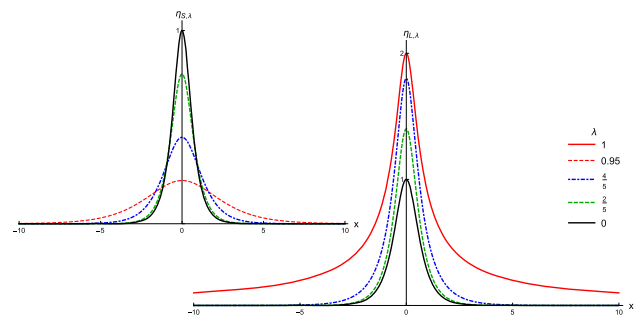

Fig. 9 The zero modes for the large kink (27) (right) and the small kink (29) (left), depicted for some values of λ. Both modes behave adequately for $\lambda \neq 1$. However, for $\lambda = 1$, we have $\eta_{S,\lambda=1} = 0$, meaning that the small topological sector disappears, while $\eta_{L,\lambda=1}(x \simeq \infty) \simeq 1/x^2$, which is a consequence of the presence of the massless meson

be written in terms of a static warped metric given by

$$ds_5^2 = g_{ab}dx^a dx^b = e^{2A(y)}ds_4^2 - dy^2. \tag{40}$$

Here $a, b = 0, ..., 4, \mu, \nu = 0, ..., 3, ds_4^2 = \eta_{\mu\nu}dx^\mu dx^\nu$, and the y-coordinate describes the extra spatial dimension. The functions $A(y)$ and $e^{A(y)}$ are called warp function and warp factor, respectively, and they are assumed to depend only on the extra dimension.

In this braneworld scenario, we are interested in models that can be described by the action

$$S = \int d^5x \sqrt{|g|} \left(-\frac{1}{4}R + \mathcal{L} \right), \tag{41}$$

where $\mathcal{L}(\phi, \partial_a \phi) = \frac{1}{2}g_{ab}\partial^a\phi\partial^b\phi - U(\phi)$ is the Lagrangian for the scalar field and, for simplicity, we assume $4\pi G_5 = 1$. We also assume that $\phi = \phi(y)$, i.e., the scalar field only depends of the extra dimension.

The Einstein equations that follow from the action (41) are

$$G_{ab} = 2T_{ab}, \tag{42}$$

where G_{ab} is the Einstein tensor and T_{ab} is the energy-momentum tensor, similar to Eq. (4). The 00 and the 44 components of (42) are given by

$$6A'^2 = \phi'^2 - 2U, \tag{43a}$$
$$3A'' + 6A'^2 = -\phi'^2 - 2U, \tag{43b}$$

respectively, with the prime denoting derivation with respect to the coordinate y. With Eq. (43) at hand we can subtract the first equation from the second to obtain

$$A'' = -\frac{2}{3}\phi'^2. \tag{44}$$

Equation (44) provides a way to rewrite the system in terms of first-order equations. For this purpose, we introduce a function $W(\phi(y))$ in the equations through the relation

$$A' = -\frac{2}{3}W(\phi(y)). \tag{45}$$

As a consequence, the equation providing the solution for the scalar field is now

$$\phi' = W_\phi. \tag{46}$$

In order to solve the equations of motion, these two first-order equations require that the potential obeys

$$U(\phi) = \frac{1}{2}W_\phi^2 - \frac{4}{3}W^2. \tag{47}$$

Equations (45) and (46) constitute the first-order framework and can be used to analyze possible scenarios of thick brane that can be generated by the models presented in the previous section.

The analysis of the thick branes scenario generated by the large kink (27) is similar to the case of small kinks (29), so we concentrate on the brane generated by the small kink. To simplify the investigation, let us perform a shift in the field, $\phi \rightarrow \phi - K_\lambda$. In this case, one gets

$$W(\phi) = \frac{\sqrt{1-\lambda}}{\lambda}\left(\frac{2\tan^{-1}(\sqrt{1-\lambda}\,\text{sc}(\phi, \lambda))}{\sqrt{1-\lambda}} \right.$$
$$\left. -(2+\lambda)\text{am}(\phi, \lambda) \right). \tag{48}$$

Due to the shift performed over ϕ, the field solution of (46) becomes

$$\phi_\lambda(y) = \text{sc}^{-1}\left(\frac{\tanh\left(\sqrt{1-\lambda^2}\,y\right)}{\sqrt{1+\lambda}}, \lambda \right). \tag{49}$$

Its shape can be observed in Fig. 3, when we make the changes $x \rightarrow y$ and $\phi_\lambda(y) = \chi_{S,\lambda}(y) - K_\lambda$. Note that, for $\lambda = 1$ the field approaches a constant, $\phi_{\lambda=1}(\pm\infty) = \pm\text{csch}^{-1}\left(\sqrt{2}\right)$.

With these ingredients we analytically solve Eq. (45), together with the boundary conditions $A(0) = A'(0) = 0$, to find

$$A(y) = -\frac{2}{3\lambda}\left[\sqrt{1-\lambda}(2+\lambda)\mathcal{F}\left(\sqrt{1+\lambda}, \sqrt{1-\lambda^2}, y\right) \right.$$
$$\left. -2\mathcal{F}\left(\sqrt{\frac{1+\lambda}{1-\lambda}}, \sqrt{1-\lambda^2}, y\right) \right], \tag{50}$$

where

$$\mathcal{F}(b, a, x) = -x\cot^{-1}(b) + \frac{i}{4a}\left[\text{Li}_2\left(\frac{b+i}{i-b}e^{2ax}\right) \right.$$
$$- \text{Li}_2\left(\frac{i-b}{b+i}e^{2ax}\right) - \text{Li}_2\left(\frac{b+i}{i-b}\right)$$
$$\left. + \text{Li}_2\left(\frac{i-b}{b+i}\right) \right]. \tag{51}$$

Here $\text{Li}_2(y)$ is the polylogarithmic function. The shape of $e^{2A(y)}$ is depicted in Fig. 10. We can observe that in the vicinity of the center the warp factor behaves like $A(|y| \simeq 0) \simeq (1 - \lambda)y^2 + \mathcal{O}(y^4)$, which implies that, as $\lambda \rightarrow 1$, the brane becomes less and less localized, becoming effectively delocalized for $\lambda = 1$. Meanwhile, in the asymptotic regime $|y| \rightarrow \infty$ the thick brane approaches AdS vacua with cosmological constant $\Lambda_5 \sim -W(\phi(\pm\infty))^2$, and we have $A(|y| \rightarrow \infty) \simeq -\frac{1}{3}E_S(\lambda)|y|$, where we used Eqs. (18) and (34). As $E_S(\lambda)$ decreases as λ grows (starting at $\lambda = 0$, where we have the sine-Gordon brane) the thick branes generated by
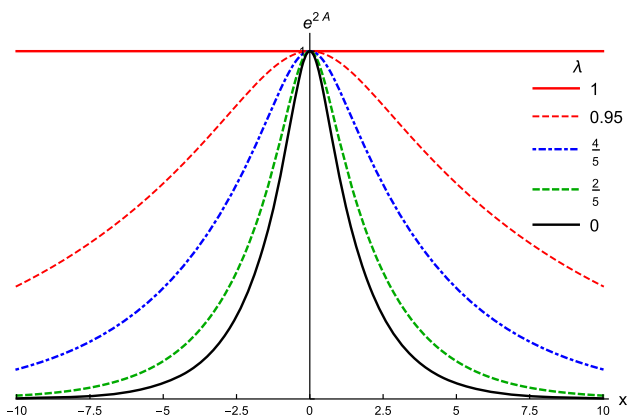
Fig. 10 The warp factor that follows from (50) for some values of λ. Here we see how it evolves from the sine-Gordon case when $\lambda = 0$ to a 5-dimensional flat spacetime when $\lambda = 1$

Fig. 11 The energy density for some values of λ. Here we see how it becomes delocalized as $\lambda \to 1$. For $\lambda = 1$, there is no more energy concentration around the origin and the brane disappears from the background geometry

this model approaches AdS vacua with smaller cosmological constant as $\lambda \to 1$. In particular, for $\lambda = 1$ the brane seems to fill the entire space, so we have no graviton localization anymore at this point, with all the modes dispersed through the extra dimension. The braneworld scenario is destroyed in the limit $\lambda \to 1$.

From Eq. (43) we find that the potential has to obey (47) and one notes that it keeps the correct form for vacuum stability in gravitational theories [34,35]. In particular, for $\lambda = 1$ the potential $U(\phi)$ vanish, and the spacetime solution reaches a flat 5-dimensional geometry. At this point, only the dynamical term $\sim \partial^a \phi \partial_a \phi$ survives in the action (41), having as solution the constants $\phi_{\lambda=1}(\pm\infty)$. The presence of two values possible for the scalar field in the flat background is due the original $\mathbb{Z}_2$-symmetry, which act as a memory related to the kind of thick brane system from which it is derived.

The energy density of the model is given by

$$\rho(y) = e^{2A} \left(W_\phi^2 - \frac{4}{3} W^2 \right), \qquad (52)$$

and its shape is depicted in Fig. 11. It is well known that models derived from the first-order equations (45) and (46) have zero energy. It happens because we can rewrite the energy density as a total derivative, $\rho(y) = \frac{d}{dy} \left(W e^{2A} \right)$. As $W(\phi(\pm\infty))$ is finite and asymptotically the warp function falls off as $e^{-constant^2|y|}$, the integral of $\rho(y)$ over all space must vanish. Here we see that when $\lambda = 0$, the energy density is well concentrated around the origin and, as λ increases, it becomes more and more diffuse, finally disappearing at $\lambda = 1$.

The above results describe an interesting scenario, in which the parameter λ may be used to control the physical properties of the 5-dimensional spacetime. If λ increases from 0 to unity, it may change the spacetime from a braneworld model with a single extra spatial dimension of
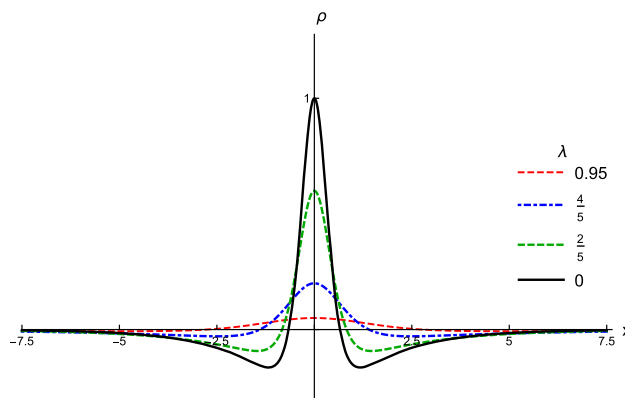
infinite extent to a 5-dimensional Minkowski spacetime with no graviton localization.

4.1 Metric fluctuations

In this section we analyze the stability of the gravitational sector. For this purpose, we perform a redefinition of variable $dy^2 \to e^{2A(z)} dz^2$ in (40), which allows us to rewrite the metric in a conformally flat scenario $\tilde{g}_{ab} = e^{2A(z)} \eta_{ab}$. With a linear perturbation the metric becomes

$$ds^2 = e^{2A(z)} (\eta_{ab} + h_{ab}) \, dx^a dx^b. \qquad (53)$$

In the transverse-traceless gauge ($\partial_\mu h^{\mu\nu} = 0$ and $h_\mu^\mu = 0$) the conformal Einstein tensor is $\bar{G}_{ab} = -\frac{1}{2} \partial_c \partial^c h_{ab}$ and the linearized Einstein tensor is given by

$$G_{ab}^{(1)} = -\frac{1}{2} \partial_c \partial^c h_{ab} + 3 \Big[\partial_a A \partial_b A - \partial_a \partial_b A \\ + \frac{1}{2} A' h'_{ab} + \bar{g}_{ab} \left(\partial_c \partial^c A + \partial_c A \partial^c A \right) \Big]. \qquad (54)$$

In this way the $\mu\nu$-components of $G_{ab}^{(1)}$ are

$$G_{\mu\nu}^{(1)} = -\frac{1}{2} \partial_c \partial^c h_{\mu\nu} + \frac{3}{2} A' h'_{\mu\nu} - 3 \bar{g}_{\mu\nu} \left(A'' + A'^2 \right), \quad (55)$$

and the linearized energy-momentum tensor becomes

$$T_{\mu\nu}^{(1)} = -\frac{3}{2} \bar{g}_{\mu\nu} \left(A'' + A'^2 \right), \qquad (56)$$

where the prime denotes the derivative with respect to the variable z. When using linearized Einstein equations, $G_{\mu\nu}^{(1)} = 2 T_{\mu\nu}^{(1)}$, we obtain the equation for $h_{\mu\nu}$, which is $-\partial_c \partial^c h_{\mu\nu} + 3 A' h'_{\mu\nu} = 0$. At last, the redefinition $H_{\mu\nu} = e^{-ipx} e^{3A/2} h_{\mu\nu}$ allows us to rewrite the equation for $h_{\mu\nu}$ as
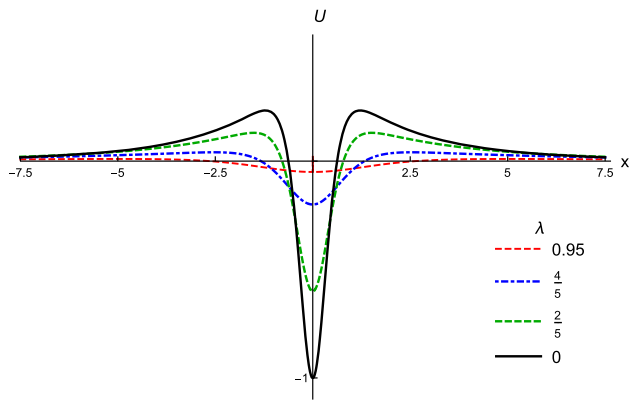
Fig. 12 The stability potential (58) for some values of λ. Here we observe that the stability potential of the gravitational sector considerably decreases when $\lambda \to 1$, although it always maintains its volcano shape, implying stability for gravity localization. For $\lambda = 1$, Eq. (58) vanishes

$$\left(\partial_z + \frac{3}{2}A'\right)\left(-\partial_z + \frac{3}{2}A'\right)H_{\mu\nu} = p^2 H_{\mu\nu}. \tag{57}$$

Note that Eq. (57) has the form of a supersymmetric Schrödinger equation, where the stability potential is

$$U(z) = \frac{3}{2}A'' + \frac{9}{4}A'^2. \tag{58}$$

It is depicted in Fig. 12. We can observe that (58) keep its volcano shape, as usual, but as λ grows it becomes less pronounced, and we have no stability potential for $\lambda = 1$. Equation (57) has the factorized form $S^+S^-\psi = p^2\psi$, where $S^\pm = \left(\pm\partial_z + 3A'/2\right)$. In particular, the zero-energy solution of (57) is given by $\psi_0(y) = e^{3A(y)/2}$, where the asymptotic behavior of $A(y)$ ensures gravity localization around the brane for $0 \leq \lambda < 1$. Since the Hermitian operator S^+S^- is non-negative, we have no normalizable negative gravitons modes, and it ensures system stability. At $\lambda = 1$, we find a flat space, so the stability analysis as presented here fails. In this case, the stability of this space is guaranteed by the positive mass theorems on asymptotically flat spacetimes, which are valid for dimensions ≤ 7 [36,37].

4.2 RG flow

As pointed out in [30,31], by rewriting the metric (40) in the form

$$ds^2 = u^2\eta_{\mu\nu}dx^\mu dx^\nu - \frac{1}{A'(y)^2}\frac{du^2}{u^2}, \tag{59}$$

where $u = e^{A(y)}$, we are allowed to interpret the function $u(y)$ as the renormalization scale of some quantum field theory in the sense of the gauge/gravity duality [26–29]. Note that, due to the boundary conditions on the deformation factor, u is limited to the range $[0, 1] = [e^{A(\pm\infty)}, e^{A(0)}]$. Thus,

domain wall solutions such as those presented here naturally lead to confining regimes with a UV-cutoff located at $u = 1$ in the dual field theory. In this context, the solution $\phi(y(u))$ is identified with the running coupling of the system (see [10,38,39] and the references therein), so that the β-function defined by

$$\beta(\phi) = u\frac{d\phi}{du} = -\frac{3}{2}\frac{W_\phi}{W} \tag{60}$$

describes the RG flow in the dual theory.

Denoting the critical points of (47) by $\phi_{\lambda,\infty}$, we can identify them with the zeros of W_ϕ, which leads to the AdS (or flat) vacua. Expanding the β-function around its critical point we have $\beta(\phi) \simeq \beta(\phi_{\lambda,\infty}) + \beta'(\phi_{\lambda,\infty})(\phi - \phi_{\lambda,\infty}) + \mathcal{O}\left((\phi - \phi_{\lambda,\infty})^2\right)$. Since in the critical points we have $\beta(\phi = \phi_{\lambda,\infty}) = 0$, we can find the following expression for the running coupling:

$$\phi = \phi_{\lambda,\infty} + cu^{\beta'(\phi_{\lambda,\infty})}. \tag{61}$$

Note that if $\beta'(\phi_{\lambda,\infty}) < 0$, $\phi_{\lambda,\infty}$ is a UV fixed point when $u \to \infty$, and if $\beta'(\phi_{\lambda,\infty}) > 0$, $\phi_{\lambda,\infty}$ is a IR fixed point for $u \to 0$. For $\beta'(\phi_{\lambda,\infty}) = 0$ we have a conformal theory.

For the model presented here, we have

$$\beta'(\phi_{\lambda,\infty}) = \frac{3\lambda\,\mathrm{cn}\left(\phi_{\lambda,\infty}, \lambda\right)\,\mathrm{sn}\left(\phi_{\lambda,\infty}, \lambda\right)}{\mathrm{am}\left(\phi_{\lambda,\infty}, \lambda\right) - \frac{2}{\sqrt{1-\lambda}(2+\lambda)}\tan^{-1}\left(\sqrt{\frac{1-\lambda}{1+\lambda}}\right)} \tag{62}$$

where $\phi_{\lambda,\infty} = \mathrm{sc}^{-1}\left(\frac{1}{\sqrt{1+\lambda}}, \lambda\right)$. Note that (62) is a monotonically increasing function of λ and we have no divergences in the running coupling since $u \in [0, 1]$, but for any λ the IR regime ($u \to 0$) at $\phi = \phi_{\lambda,\infty}$ is well defined in the dual field theory, even for the 5d Minkowski setup. As a consequence, none of the solutions has a conformal dual field theory.

5 Comments

In this work we studied a sine-Gordon-like model, which is controlled by a real parameter that continuously connects the sine-Gordon and the vacuumless models. The model appears as a deformation of the ϕ^4 model, and the real parameter is λ: for $\lambda = 0$ one gets the standard sine-Gordon model and for $\lambda = 1$ it reproduces the so-called vacuumless model. However, for λ in the interval $(0, 1)$ one gets a double sine-Gordon model, which contains two distinct topological sectors, the large and the small sectors, which give rise to large and small kinks, respectively.

As shown, in the 2-dimensional spacetime, the energy of the large kink in the large sector varies from $E_L(\lambda = 0) = 1$

to $E_L(\lambda = 1) = 2\pi$, and in the case of the small sector one gets $E_S(\lambda = 0) = 1$ and $E_S(\lambda = 1) = 0$. We then see that the small sector, which is degenerate with the large sector at $\lambda = 0$, disappears as $\lambda = 1$, with the large sector becoming the topological sector of the vacuumless model.

In the 5-dimensional case, we considered a warped geometry with a single extra dimension of infinite extent and studied the new braneworld scenario described in the small sector. In this scenario, the brane energy density is such that the brane energy vanishes, independently of the value of λ. If we see the model with λ increasing from zero to unity, it then nicely describes a way to change a 5-dimensional warped geometry which is asymptotically AdS into a 5-dimensional Minkowski geometry. However, if λ is supposed to run in the reverse sense, decreasing from unity to zero, the model could do the reverse, changing the 5-dimensional Minkowski geometry into a braneworld scenario with a warped geometry which is asymptotically AdS$_5$.

As we have shown, the model is stable under tensorial fluctuations in the metric and of current interest, so one should now investigate how it modifies Newton's law, and how fermion and gauge fields can be entrapped into the brane as λ varies in the interval $[0, 1]$. Another issue of current interest concerns the variation of λ: the present investigation cannot tell the value of λ, so one should search for this considering other arguments. An interesting possibility is to investigate the conformational entropy associated with the current braneworld model, and see how it behaves as λ varies in the interval $[0, 1]$. This has been recently investigated in other contexts in [40–43] and in the references therein, and it may provide an important guide towards the physical realization of gravity localization in the present model, since the entropy could perhaps suggest a better way λ should vary, increasing or decreasing in the interval $[0, 1]$.

References

1. A. Vilenkin, E.P.S. Shellard, *Cosmic Strings and Other Topological Defects* (Cambridge University Press, Cambridge, 1994)
2. N.S. Manton, P. Sutcliffe, *Topological Solitons* (Cambridge University Press, Cambridge, 2004)
3. T. Vachaspati, *Kinks and Domain Walls: An Introduction to Classical and Quantum Solitons* (Cambridge University Press, Cambridge, 2006)
4. P.J. Caudrey, J.C. Eilbeck, J.D. Gibbon, Il Nuovo Cimento B **25**, 497 (1975)
5. I. Cho, A. Vilenkin, Phys. Rev. D **59**, 021701 (1999)
6. I. Cho, A. Vilenkin, Phys. Rev. D **59**, 063510 (1999)
7. D. Bazeia, Phys. Rev. D **60**, 067705 (1999)
8. D. Bazeia, F.A. Brito, J.R.S. Nascimento, Phys. Rev. D **68**, 085007 (2003)
9. A. de Souza Dutra, A.C. Amaro de Faria Jr., Phys. Rev. D 72, 087701 (2005)
10. D. Bazeia, F.A. Brito, L. Losano, JHEP **0611**, 064 (2006)
11. D. Bazeia, F.A. Brito, F.G. Costa, Phys. Lett. B **661**, 179 (2008)
12. D. Bazeia, L. Losano, J.M.C. Malbouisson, Phys. Rev. D **66**, 101701 (2002)
13. L. Randall, R. Sundrum, Phys. Rev. Lett. **83**, 4690 (1999)
14. L. Randall, R. Sundrum, Phys. Rev. Lett. **83**, 3370 (1999)
15. W.D. Goldberger, M.B. Wise, Phys. Rev. Lett. **83**, 4922 (1999)
16. O. DeWolfe, D.Z. Freedman, S.S. Gubser, A. Karch, Phys. Rev. D **62**, 046008 (2000)
17. C. Csaki, J. Erlich, T.J. Hollowood, Y. Shirman, Nucl. Phys. B **581**, 309 (2000)
18. M. Gremm, Phys. Lett. B **478**, 434 (2000)
19. G. Dvali, G. Gabadadze, M. Porrati, Phys. Lett. B **485**, 208 (2000)
20. D. Bazeia, D.C. Moreira, Phys. Lett. B **748**, 79 (2015)
21. D. Bazeia, M.A. Marques, R. Menezes, D.C. Moreira, Ann. Phys. **361**, 574 (2015)
22. D. Bazeia, M.A. Marques, R. Menezes, Phys. Rev. D **92**, 084058 (2015)
23. D. Bazeia, R. Menezes, Roldao da Rocha, Adv. High Energy Phys. **2014**, 276729 (2014)
24. R. Menezes, D.C. Moreira, Ann. Phys. **383**, 662 (2017)
25. F.A. Brito, M. Cvetic, S.-C. Yoon, Phys. Rev. D **64**, 064021 (2001)
26. J.M. Maldacena, Adv. Theor. Math. Phys. **2**, 231 (1998)
27. J.M. Maldacena, Int. J. Theor. Phys. **38**, 1113 (1999)
28. S.S. Gubser, I.R. Klebanov, A.M. Polyakov, Phys. Lett. B **428**, 105 (1998)
29. E. Witten, Adv. Theor. Math. Phys. **2**, 253 (1998)
30. H.J. Boonstra, K. Skenderis, P.K. Townsend, JHEP **9901**, 003 (1999)
31. K. Skenderis, P.K. Townsend, Phys. Lett. B **468**, 46 (1999)
32. E.B. Bogomol'nyi, Sov. J. Nucl. Phys. **24**, 449 (1976)
33. M. Prasad, C. Somerfield, Phys. Rev. Lett. **35**, 760 (1975)
34. P.K. Townsend, Phys. Lett. B **148**, 55 (1984)
35. W. Boucher, Nucl. Phys. B **242**, 282 (1984)
36. M. Eichmair, L.-H. Huang, D.A. Lee, R.M. Schoen, J. Eur. Math. Soc. **18**, 83 (2016)
37. R.M. Schoen, S.T. Yau, Proc. Natl. Acad. Sci. USA **76**, 1024 (1979)
38. E. Kiritsis, W. Li, F. Nitti, Fortsch. Phys. **62**, 389 (2014)
39. E. Kiritsis, F. Nitti, L.S. Pimenta, Fortsch. Phys. **65**, 1600120 (2017)
40. R.A.C. Correa, A. de Souza Dutra, M. Gleiser. Phys. Lett. B **737**, 388 (2014)
41. R.A.C. Correa, D.M. Dantas, C.A.S. Almeida, R. da Rocha, Phys. Lett. B **755**, 358 (2016)
42. A.E. Bernardini, N.R.F. Braga, R. da Rocha, Phys. Lett. B **765**, 81 (2016)
43. N.R.F. Braga, R. da Rocha, Phys. Lett. B **767**, 381 (2017)